

Iododeoxyuridine Uptake and Retention as a Measure of Tumor Growth

J. Tjuvajev, A. Muraki, J. Ginos, J. Berk, J. Koutcher, D. Ballon, B. Beattie, R. Finn and R. Blasberg

Cotzias Neuro-Oncology Laboratory and Department of Radiology, Memorial Sloan Kettering Cancer Center, New York, New York and Department of Radiology, Valley General Hospital, Monroe, Washington

Iodine-131-iododeoxyuridine (IUdR) uptake and retention was measured in two C6 glioma cell lines (C6_m and C6_a) with different growth characteristics. Animals with intracerebral (i.c.) C6_a tumors had a mean survival of 16 days, whereas only 1 of 20 animals with i.c. C6_m tumors died during an 8-wk period of observation. The growth of i.c. C6_m tumors could be described by the Gompertz equation; tumor doubling time increased from 1.9 to 5.2 days between Days 8 and 16 after tumor inoculation. Corresponding measurements of ¹³¹I-IUdR uptake and retention (24 hr after IUdR administration) by i.c. C6_m tumors were also time-dependent and decreased from 0.075 to 0.027 to 0.011 %dose/g in 8-, 10- and 16-day-old tumors, respectively. Iodine-131-IUdR uptake in "rapidly growing" i.c. C6_a tumors was substantially higher (0.30 %dose/g at 24 hr) than that in "slowly growing" i.c. C6_m tumors and corresponded with differences in the survival data. Subcutaneous C6_a tumors had comparable high uptake values (0.49 %dose/g at 24 hr), and 93% of total tumor radioactivity was recovered in DNA 24 hr after IUdR administration. Clearance of radioactivity was rapid in nonproliferative tissues; more than 80% of plasma radioactivity was cleared in 24 hr. Tumor-to-cortex radioactivity ratios ranged from 100/1 to 120/1 and 150/1 between 24, 48 and 96 hr after IUdR injection respectively. A "washout strategy," which reduces tissue background activity and increases specificity for PET and SPECT imaging of IUdR-DNA incorporation, is possible with longer-lived radioisotopes of iodine.

J Nucl Med 1993; 34:1152-1162

Anoninvasive measure of tumor cell proliferation could aid in selecting specific therapies and could provide a much earlier indication of a response to therapy than images of tumor volume or glucose metabolism. Changes in tumor volume observed on computed tomography (CT) or magnetic resonance (MR) images and changes in apparent glucose metabolism observed on fluorodeoxyglucose positron emission tomography (PET) scans following therapy have been shown to take weeks to months (1-6). The potential for obtaining functional images of DNA synthesis using

PET and single-photon emission computed tomography (SPECT) has been recognized for some time (7-9). PET and SPECT provide the opportunity to perform dynamic measurements of uptake, distribution and clearance of radiolabeled precursors of DNA in both tumors and normal tissues of patients with cancer. Our interest in halogenated pyrimidines to image tumor proliferation developed because iododeoxyuridine (IUdR) has been shown to be incorporated into DNA of dividing cells and because radioisotopes of iodine are available for both PET and SPECT imaging that have comparatively long half-lives. This permits imaging after clearance or "washout" of radiolabeled metabolites not incorporated into DNA. IUdR is an analog of thymidine, it is phosphorylated by thymidine kinase and incorporated into DNA in place of thymidine. Although IUdR is incorporated into tissue DNA with a lower efficiency than thymidine (10), our proposed use of iodine-labeled IUdR is substantially different from other investigations which use ¹¹C-thymidine (TdR) or ¹⁸F-fluorodeoxyuridine (FUDR). Previous studies have demonstrated that substantial incorporation of ¹²⁵I-IUdR into DNA occurs in proliferating tissue (tumor and intestine), that it is retained with a slow rate of clearance and that low background radioactivity is observed 1 to 4 days after intravenous administration in animals (11-20). Clearance of background radioactivity following intravenous administration of *I-IUdR is rapid because iodide is the major radiolabeled metabolite of *I-IUdR and iodide is rapidly cleared by the kidney (11,13,21,22). The comparatively long physical half-lives of ¹²⁴I (4.2 days), ¹³¹I (8.1 days) and ¹²³I (13 hr) are appropriate for the longer IUdR experiments we propose for PET and SPECT imaging.

A goal of this study was to investigate the feasibility of using IUdR for imaging tumor cell proliferation. We demonstrated a relationship between ¹³¹I-IUdR uptake after intravenous administration and the volumetric growth rate of intracerebral (i.c.) C6_m tumors and a relationship between ¹³¹I-IUdR uptake and animal survival by comparing two tumors (C6_m and C6_a) with different growth characteristics. We also measured the fraction of tumor radioactivity that is incorporated into DNA 24 hr after administration of ¹³¹I-IUdR and utilized a delayed sampling strategy to facilitate washout of radiolabeled metabolites in order to increase specificity and increase the tumor-to-background

Received Nov. 12, 1992; revision accepted Mar. 31, 1993.

For correspondence or reprints contact: Ronald G. Blasberg, MD, Dept. of Neurology, Rm. C799, Memorial Sloan Kettering Cancer Center, 1275 York Ave., New York, NY 10021.

TABLE 1
Summary of Studies

Study	Group	C6 glioma	Animal host (strain)	Number of animals	Day after tumor inoculation
Survival	Group A	C6 _m	Wistar	20	—
	Group B	C6 _a	Wistar	20	—
	Group C	C6 _a	Wistar-Furth	15	—
Growth rate		C6 _m	Wistar	22	10–28
IUdR	Group I	C6 _m	Wistar	10	16
	Group II	C6 _m	Wistar	5	10
	Group III	C6 _m	Wistar	14	8
	Group IV	C6 _a	Wistar	12	11
	Group V	C6 _a	Wistar-Furth	10	10

ratio. Finally, we demonstrate that the “apparent” clearance of IUdR incorporated into DNA of 8-day-old C6_m i.c. tumors can be explained by continued growth of the tumor (increase in tumor volume) during the interval between measurements of tumor radioactivity (%dose/g tissue).

MATERIALS AND METHODS

Cell Culture

The C6 clone was originally obtained from an N-nitrosomethylurea induced glioma (23,24). Two C6 cell lines were maintained in our laboratory. One cell line was obtained from the Memorial Sloan Kettering Cancer Center tissue culture bank (C6_m) and one cell line was obtained from the American Tissue Culture Collection (C6_a). C6 cells were grown as monolayers in T-150 flasks (Falcon) in F-10 media with 17.5% fetal calf serum. The cultures were maintained in an incubator with 5% CO₂, 80% humidity at 37°C. Cells were passaged each week or used for implantation after having become 90% confluent.

Tumor Implantation

Single C6 cell suspensions for implantation were prepared from cell culture monolayers by incubation in an 0.05% trypsin solution for 1–2 min at 37°C. The cells were resuspended in 10 ml of fresh media, pelleted and resuspended in a small volume of fresh media to obtain 10⁵ cells in 10 μl of suspension. The cell suspension was aspirated into a 100-μl gas tight Hamilton syringe (Ga.25) and attached to a stereotaxic device. Male outbred Wistar and inbred Wistar-Furth rats weighing 250 ± 20 g were anesthetized with a gas mixture consisting of 1.5% fluothane, 70% nitrous oxide and 30% oxygen. A 2% lidocaine gel was applied to the ears and the head was fixed in a stereotaxic device. After midline scalp incision, a burr hole was made through the skull 1 mm in front of the coronal suture and 3 mm to the right of the midline. The syringe needle was then slowly lowered 5 mm into the frontal lobe and 10 μl of the tumor cell suspension containing 10⁵ cells were injected over 2 min. Bone wax was applied to cover the skull defect and the scalp was closed with 4.0 silk suture. To produce both intracerebral and subcutaneous C6 tumor-bearing animals, an additional 100 μl of the tumor cell suspension (10⁶ cells) was injected subcutaneously in the dorsal thoraco-cervical region using a tuberculin syringe. After the procedure, the animals were marked and placed in standard cages with water and Rodent LabChow #5001 (Purina Mills, Inc.) ad libitum.

Survival Study

Five separate survival studies were performed (Table 1). Two groups of 10 outbred Wistar rats were inoculated with 10⁵ C6_m tumor cells (data combined, Group A). Two additional groups of 10 outbred Wistar rats (data combined, Group B) and one group of 15 inbred Wistar-Furth rats (Group C) were inoculated with 10⁵ C6_a tumor cells to compare survival in two different strains of Wistar rats. The animals were observed daily and when they developed symptoms of ataxia, paresis, seizures or a 20% weight loss, they were interpreted as being “near death” and the animal was euthanized with intraperitoneal phenobarbital (120 mg/kg) to avoid further distress. Life expectancy of the “near death” animals was estimated to be 1 day or less. The day of euthanasia was treated as the day of death in plotting the survival curves.

MRI Monitoring of Tumor Growth

Three separate groups of Wistar rats (total of 22 animals) were injected intracerebrally with 10⁵ C6_m tumor cells as described above. Two or three sequential MR scans were performed at 3–4-day intervals on each animal 10–28 days following i.c. injection of tumor cells. MRI was performed on a whole-body 1.5 Tesla (G.E. Signa) scanner. A specially designed small volume solenoid resonator was used to obtain the images utilizing standard T1-weighted spin-echo sequences. A sagittal localizer was obtained utilizing a T1-weighted spin-echo sequence (TR 500 msec; TE 30 msec; with two excitations per phase encoding step, with 3-mm thick slices and a gap of 1 mm between slices); a field of view of 80 mm and a matrix of 128 × 256 was utilized. Afterwards, coronal images were obtained with a similar pulse sequence using four excitations per phase encoding step.

The tumor-bearing rats were anesthetized with a mixture of ketamine 60 mg/kg and acetylpromazine 2.5 mg/kg i.p. Imaging was performed within 5 min of the contrast injection (Gd/DTPA; 0.2 ml/per kg, i.v.). The enhanced tumor area on each slice was measured utilizing a proprietary GE software package (Signa). The summed areas were multiplied by the sum of slice thickness and interslice gap (4 mm) to obtain the total volume of tumor (mm³). MRI volume measurements in studies of cerebral infarction (25) and metastatic tumor to liver (26) were shown by us to correlate well with morphological volume measurements.

Synthesis and Purification of IUdR

No-carrier-added IUdR was prepared by allowing an excess of 2'-deoxyuridine (IUdR) (Aldrich Chem. Co., St. Louis, MO) to

react with a buffered solution of [^{131}I]NaI (Du Pont), ranging from 222 to 407 MBq (6.0 to 11.0 mCi) in a vial coated with Iodogen (Sigma Chem. Co., St. Louis, MO). The reaction solution was purified by elution through a Sep Pak C18 cartridge (Waters). The eluted fraction containing IUdR was evaporated under high vacuum with mild heating, and the residue was dissolved in a sterile, pyrogen-free saline solution prior to injection. Radiochemical purity was >99%; HPLC analysis using an ultraviolet detector showed the presence of trace amounts of UdR (9–24 μg) in our preparations yielding 12–18 mCi of IUdR. Under worst case conditions, this represents <0.7 μg UdR/animal. The mass of IUdR in the ^{131}I -IUdR preparation was detected by ultraviolet spectroscopy at a wave length of 288 nm. Specific activities of 1700 and 560 Ci/mmol were obtained from starting ^{131}I -iodide specific activities of 1840 and 1300 Ci/mmol, respectively. Radiochemical yield following purification ranged from 72% to 82%.

IUdR Animal Studies

Prior to ^{131}I -IUdR administration, animals were given daily intraperitoneal injections (1 ml of 0.9% NaI solution) for a period of 3–4 days to block thyroidal and tissue uptake of ^{131}I -iodide and to decrease the plasma protein iodination resulting from dehalogenation of ^{131}I -IUdR. IUdR uptake and retention experiments were performed by administering 9.25 or 14.8 MBq (250 or 400 μCi) of ^{131}I -IUdR in 1 ml of saline as an intravenous injection into the tail vein over 30 sec. Animals were killed by decapitation at various time points after administration of ^{131}I -IUdR: 1, 24, 48, 96 and 120 hr. Throughout this paper, time in *hours* will refer to the time after ^{131}I -IUdR administration and time in *days* will refer to the time after tumor cell inoculation. Brain tumor and tumor-free brain in the contralateral hemisphere, subcutaneous tumor in animals bearing both i.c. and subcutaneous tumors, various organ tissues, blood and plasma were sampled, weighed and counted in a Packard 5500 Gamma Spectrometer. Decay-corrected radioactivity was expressed as a percentage of the administered dose per gram of tissue.

Assay for IUdR Incorporated into DNA

Subcutaneous tumor samples were dissected, weighed (100–150 mg) and cooled to 4°C, after which 250 μl of cold phosphate-buffered saline (PBS) was added and the mixture was homogenized by an ultrasonic cell disrupter (Branson Sonifier II, Baxter). Approximately half of the tissue homogenate was weighed and counted by gamma spectroscopy. To the remaining tissue homogenate, 250 μl of 20% trichloroacetic acid (TCA) was added and incubated for 30 min at 50°C to remove the acid-soluble fraction of metabolites. The precipitate was washed twice with 10% TCA, reweighed and resuspended in standard PBS. The TCA insoluble precipitate includes protein, RNA and DNA fractions (16,27). To confirm radioactivity in DNA, the acid-insoluble precipitate was incubated in a 0.75-ml Ringers stabilized buffer (RSB) solution containing 250 $\mu\text{g}/\text{ml}$ proteinase K and 10% SDS at 37°C for 3–4 hr or until the pellet is completely dissolved. One-tenth milliliter of 5 M NaCl was added followed by 0.75 ml of SS-phenol:chloroform:isoamyl alcohol (10:10:1). After mixing and brief centrifugation for phase separation, the aqueous phase was removed and placed in a new vial. To obtain complete DNA extraction, two aqueous phase washes (0.75 ml RSB buffer plus 0.1 ml 5 M NaCl) were performed. The aqueous phase extract and aqueous washes were mixed with two volumes of diethyl ether; the ether phase was aspirated and counted. Finally, 2.5 volumes of prechilled absolute ethanol was added to the aqueous phase to precipitate DNA. After centrifugation, the supernatant was re-

moved and counted. The pellet was washed twice with prechilled absolute ethanol and finally with PBS, resuspended in 1 ml of PBS with 10 mg/ml of DNase-free RNase and incubated at 37°C for 3 hr. In order to hydrolyze remaining RNA or RNA fragments, 9 M KOH was added to the solution to obtain a final concentration of 1 M and subjected to further incubation for 2 hr at 37°C. The RNA hydrolysate was extracted twice with chloroform/phenol (1:1 v/v) in the same way as the phenol extraction. DNA in the aqueous phase was precipitated with five volumes of prechilled 10% TCA and the DNA pellet washed with methanol and counted by gamma spectroscopy. The measured radioactivity was decay corrected and expressed as a fraction of acid precipitable radioactivity and as the percent of administered dose per gram of tissue.

Assay for Radiolabeled Metabolites in Plasma

Arterial blood samples were drawn at various times (0–60 min) after ^{131}I -IUdR administration and plasma was obtained. The plasma (20 μl) was counted by gamma spectroscopy (Packard Inc.) and 50 μl was treated with a 5-fold volume (w/v) of 10% TCA, cold-centrifuged at 12,000 \times g for 5 min (16,27), and 50 μl of the supernatant was used for HPLC analysis and determination of radiolabeled metabolites. HPLC procedures were performed using a HPXL solvent delivery system (Rainin Instrument Co. Inc.) and a Flo One Beta detector (Radiomatic) equipped with a 100- μl gamma cell. Metabolite separation was accomplished with a 10-micron 250 \times 4.6 mm reverse-phase C18 column (Phenomenex). The isocratic mobile phase consisted of 15% methanol in water and a flow rate of 2 ml/min was used. The time of iodide, iodouracil and IUdR elution by HPLC was independently verified by use of appropriate radiolabeled standards. Data were collected and analyzed using Dynamax software (Rainin Instrument Co. Inc.). The integrated peaks of radioactive metabolites were expressed as a percent of administered dose per milliliter of plasma.

RESULTS

Survival Studies

Outbred Wistar rats with i.c. C6_m tumors (Group A, Table 1) had prolonged survival; only 1 of 20 animals died over the 10-wk period of observation (Fig. 1). In contrast, the median survival of outbred Wistar and inbred Wistar-Furth rats with i.c. C6_a tumors was 15 and 17 days, respectively (Group B and Group C animals in Table 1 and Fig. 1, respectively). The difference in survival between Wistar and Wistar-Furth rats was not significant. These results suggest that i.c. C6_a tumors have a substantially higher growth rate than C6_m tumors.

Tumor Growth of Intracerebral C6_m Tumors

The volume of i.c. C6_m tumors was measured 10–28 days after tumor cell inoculation in 22 Wistar rats using MRI techniques (Fig. 2). Two sequential measurements of tumor volume were performed in 10 animals, and three sequential measurements of tumor volume were obtained in the other 12 animals. Tumor volume versus time after i.c. inoculation was plotted for each of the animals in the latter group; the three point plot was near linear in 3/12, slightly concave downward in 6/12, slightly concave upward in 1/12 and near exponential (upward) in 2/12. A composite of all volume measurements obtained in the 22 animals is shown in Figure 3. Mean tumor volume is plot-

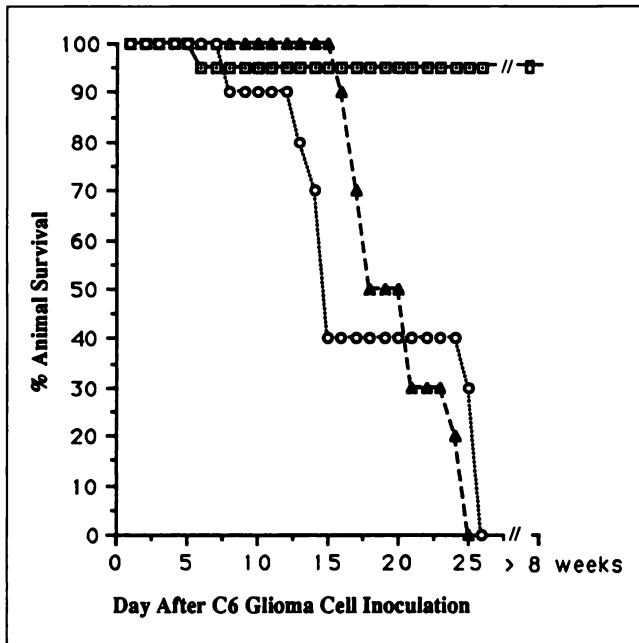


FIGURE 1. Survival after intracerebral inoculation of 10^5 C6_a and C6_m tumor cells. Group A: C6_m tumor cells in Wistar rats (open squares, n = 20); Group B: C6_a tumor cells in Wistar rats (open triangles, n = 20); Group C: C6_a tumor cells in Wistar-Furth rats (open circles, n = 15). The difference in survival between Group B and C animals was not significant.

ted versus time after i.c. inoculation. These data were fitted to the Gompertz equation (28,29) and a reasonably good fit was obtained, yielding values of 1.27 days^{-1} and 0.125 days^{-1} for coefficients A and B of the equation. The calculated initial doubling time was 0.55 days (see legend to Fig. 3).

Tumor growth rate was calculated for individual animals as the percent change in tumor volume per day and mean tumor growth rate is plotted against time after i.c. tumor inoculation in Figure 4. A time-dependent decrease in tumor growth rate was observed. The dotted curve represents the change in growth rate predicted by the estimated parameters of the Gompertz equation described above (see legend to Fig. 4). The animals in this study are comparable to Group A in the survival study (Fig. 1) and to Groups I-III in the ^{131}I -IUdR study (Tables 1 and 2). The growth rate of i.c. C6_a tumors was not determined.

IUdR Uptake and Retention in C6_m Intracerebral Tumors

The difference in uptake and retention of IUdR observed among animals studied at 16 days (Group I), 10 days (Group II) and 8 days (Group III) following C6_m inoculation was highly significant ($p = 0.001$, ANOVA; Table 2 and Fig. 5). The post-tumor inoculation time-dependent difference in IUdR uptake and retention can be related to the time-dependent changes in tumor doubling time and growth rate of animals with i.c. C6_m tumors (Table 2). Washout of radioactivity between 1 and 24 hr after ^{131}I -IUdR administration was substantially greater in Group I than in Group III animals (Fig. 5), suggesting that IUdR incorporation into DNA was markedly lower in 16-day C6_m i.c. tumors than in 8-day tumors, despite the observation that total tumor radioactivity was nearly the same in both groups at 1 hr.

IUdR Uptake and Retention in C6_a Intracerebral and Subcutaneous Tumors

Twenty-four hours after ^{131}I -IUdR administration, the retention of IUdR-derived radioactivity in 10-day and 11-

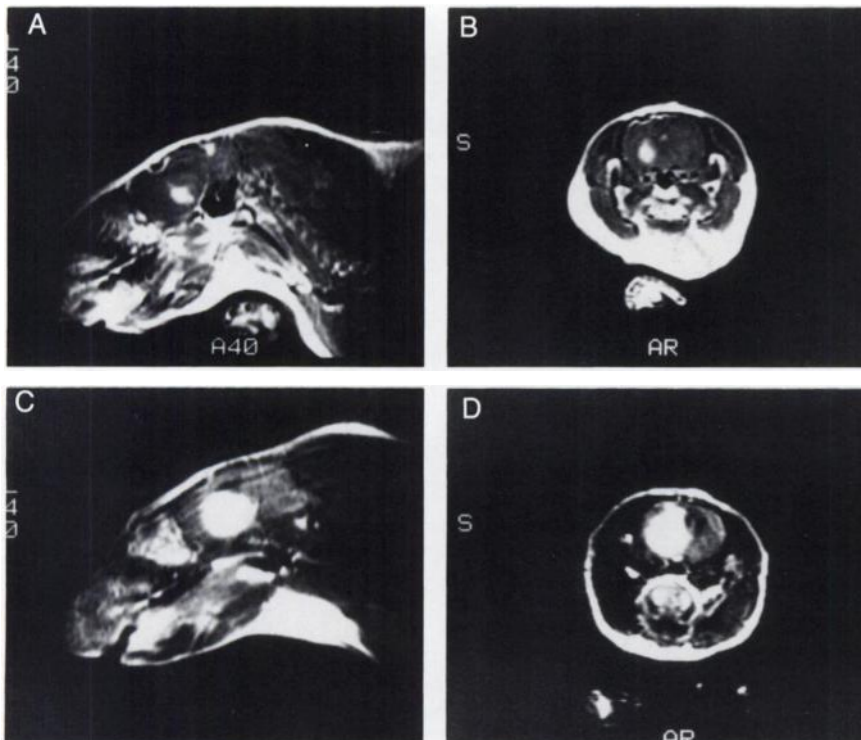


FIGURE 2. Contrast enhanced MR images of C6_m intracerebral tumors. Gd-DTPA enhanced T1-weighted MR scans were performed 8 days (A, B) and 16 days (C, D) after intracerebral inoculation of 10^5 C6_m cells. There is a significant increase in tumor size between Day 8 and Day 16 after tumor inoculation as seen on sagittal (A, C) and coronal (B, D) images. C6_m intracerebral gliomas have a distinct tumor-brain border on Gd-DTPA enhanced T1-weighted images that facilitates reasonably accurate estimates of tumor volume.

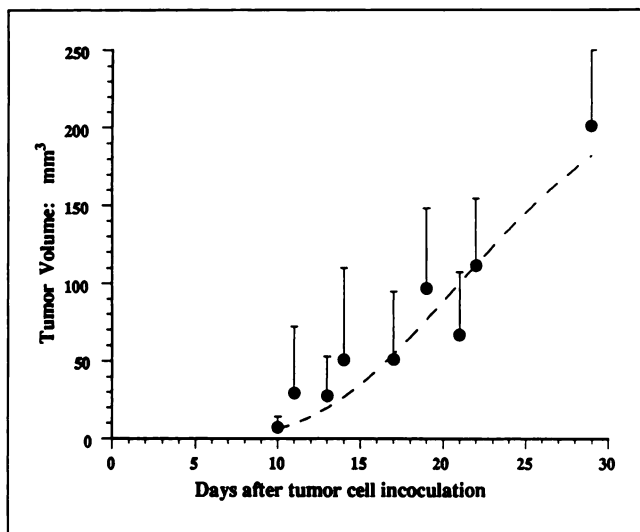


FIGURE 3. Volume measurements of intracerebral C6_m tumors. Tumor volume was determined from the contrast enhancing regions of MR images at various times after intracerebral inoculation of 10⁵ C6_m tumor cells as described in Methods. Mean values, ±s.d. (vertical bars), are plotted against time. The mean values were fitted to the Gompertz equation (28,29): $V_t = V_0 \exp \left[\frac{A}{B} * \{1 - \exp(-B * t)\} \right]$, where V_t is the tumor volume at time t , V_0 is the initial tumor volume, t is time after tumor cell inoculation and A and B are coefficients of the equation. In performing the fit, each data point was weighted by the inverse of the standard deviation of the volume measurements. The values of A and B were estimated to be $1.27 \pm 0.11 \text{ days}^{-1}$ and $0.125 \pm 0.013 \text{ days}^{-1}$; V_0 was taken to be 0.01 mm^3 . The initial doubling time is given by $[\ln(2)/A]$ and was calculated to be 0.55 days.

day i.c. C6_a tumors was significantly greater than that in 8-day i.c. C6_m tumors ($p < 0.005$, two-tailed t-test; Fig. 5 and Table 2). There was no significant difference in Wistar and Wistar-Furth animals with C6_a tumors (Groups IV and V, respectively; Table 1). Mean values from these two studies at 24, 48 and 96 hr after ¹³¹I-IUdR administration were 0.30 ± 0.20 (s.d.), 0.27 ± 0.13 , and 0.11 ± 0.08 percent dose/g tumor.

Subcutaneous tumors demonstrated essentially the same

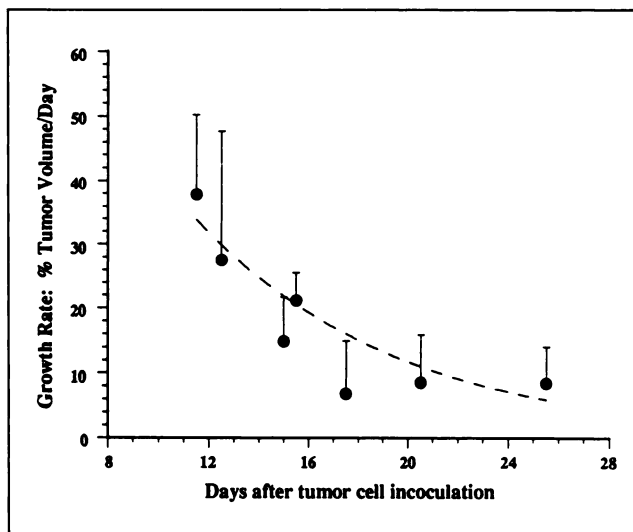


FIGURE 4. Change in volume growth rate of intracerebral C6_m tumors. Growth rate was calculated from sequential MRI measurements of tumor volume (V) after intracerebral inoculation of 10⁵ C6_m tumor cells: growth rate = percent change in tumor volume per day = $100 [2 * (V_2 - V_1)/(V_2 + V_1)] / (t_2 - t_1)$. Mean values, ±s.d. (vertical bars) are plotted against time (t) in days: $t = (t_1 + t_2)/2$. The curve is based on the Gompertz equation and the coefficients A and B estimated in Figure 3. Growth Rate = $100 [A * \exp(B * t)] / \ln(2)$.

level of IUdR uptake as i.c. tumors 24 hr after ¹³¹I-IUdR administration (Fig. 6). This similarity was maintained at 48 and 96 hr.

IUdR Incorporation into Tumor DNA

The fraction of ¹³¹I radioactivity incorporated into DNA 24 hr after ¹³¹I-IUdR administration was determined in C6_a subcutaneous tumors. Decay-corrected radioactivity in the DNA pellets was expressed as a %dose/g tumor tissue used in the extraction process and compared with values of total radioactivity in the starting tissue (Table 3). Approximately 93% of total tumor radioactivity was recoverable in DNA 24 hr after ¹³¹I-IUdR administration. The remaining 7% could be explained by radiolabeled metabolites in plasma

TABLE 2
Growth Rate and IUdR Uptake and Retention in Intracerebral C6 Tumors

Tumor cell line	Tumor cell line			
		C6 _m	C6 _a	
Study group	III	II	I	IV,V
Day of IUdR injection after tumor cell inoculation	8	10	16	10-11
Median survival*	>28	>28	>28	16
Tumor doubling time†	1.9	2.4	5.2	—
Tumor growth rate‡	52	41	19	—
Tumor activity§	0.075 ± 0.002	0.027 ± 0.008	0.011 ± 0.001	0.30 ± 0.20
Number of animals¶	4	2	3	4

*Days.

†Calculated from the Gompertz equation and fit of the volume growth plot of i.c. C6_m tumors (see Fig. 3).

‡Percent tumor volume/day; calculated from the Gompertz equation and fit of the volume growth plot of i.c. C6_m tumors (see Fig. 4).

§Iodine-131 radioactivity (%dose/g tumor) measured 24 hr after ¹³¹I-IUdR administration; mean ± s.d.

¶Number of animals used for the 24-hr ¹³¹I radioactivity measurements.

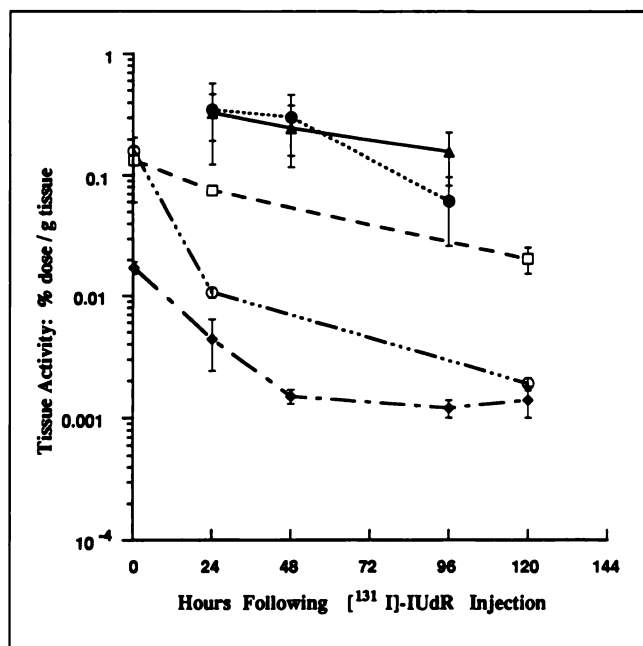


FIGURE 5. Uptake and retention of ^{131}I -IUdR derived radioactivity in i.c. C6_a and C6_m brain tumors of different age and in normal cortex. Mean values, \pm s.d. of tissue radioactivity, expressed as %dose per gram of tissue, are plotted against time after intravenous injection of ^{131}I -IUdR. Animals with i.c. C6_a tumors received ^{131}I -IUdR on postinoculation Day 11 (closed circle, Group IV) and Day 10 (closed triangle, Group V). Animals with i.c. C6_m tumors received ^{131}I -IUdR on Day 8 (open square, Group III) and Day 16 (open circle, Group I). Mean values for cortex for all groups (I–V) are shown for reference (closed triangle).

(predominantly iodide and iodinated plasma proteins at 24 hr) that equilibrate with a 20%–30% extracellular space in the tumor.

Plasma IUdR and Radiolabeled Metabolites

The kinetics of ^{131}I -IUdR clearance from blood and the appearance of radiolabeled metabolites in plasma was evaluated over 60 min after intravenous injection in six animals. Total plasma radioactivity was measured and the acid-soluble (10% TCA) fraction of plasma was assayed by HPLC. Peaks corresponding to radiolabeled iodide, iodouracil and parent IUdR were identified. Plasma radioactivity over the first 10 min was predominantly due to ^{131}I -IUdR (Fig. 7). At approximately 10 min, the concentrations of ^{131}I -IUdR and ^{131}I -iodide were equal. After 20 min, radiolabeled iodide accounts for more than 80% of total radioactivity, and the low level of iodouracil exceeds that of IUdR. The clearance of total plasma ^{131}I radioactivity from 1 to 120 hr (5 days) after ^{131}I -IUdR administration was not statistically different among the four studies (Groups I–V). Therefore, all studies were combined and mean plasma values between 1 and 120 hr were fitted to the sum of two exponentials (Fig. 6). Ninety-eight percent of plasma radioactivity was cleared with a half-time of 8.7 hr and largely represents the clearance of plasma iodide. The more slowly clearing fraction (2%) had a clearance half-time of 110 hr (4.6 days) and largely represents the acid-

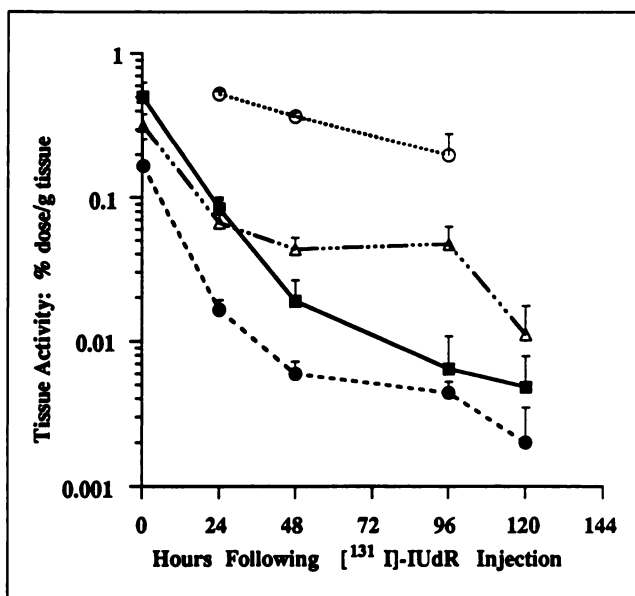


FIGURE 6. Uptake and retention of ^{131}I -IUdR derived radioactivity in subcutaneous C6_a tumors and other tissues. Mean values, \pm s.d. of tissue radioactivity, expressed as %dose/g of tissue, are plotted against time after intravenous injection of ^{131}I -IUdR. Animals with subcutaneous C6_a tumors (open circle) have been combined for clarity of presentation (Groups IV and V). Iodine- ^{131}I -IUdR was administered on post-inoculation Day 10 or 11. Values for muscle (solid circle), lung (open triangle) and plasma (closed square) were similar for all groups (I–V). They have been combined and are shown for comparison.

insoluble plasma fraction of iodinated protein. Very similar results have been shown by others (14,18,30–32).

IUdR Uptake and Retention in Systemic Tissues

IUdR uptake and retention was measured in different organs. Individual organ values varied but they were similar across study groups (Groups I–V; Figs. 5 and 6). Despite the limited amount of time-activity data between 24 and 120 hr after ^{131}I -IUdR injection, mean experimental values were fitted to a single exponential and the extrapolated activity at 0 time (A_0) and the clearance half-time ($t_{1/2}$) were determined. A 2.5-fold to 7-fold difference between the measured tissue activity at 1 hr and A_0 is shown in Table 4. This difference (1 hr value $> A_0$) indicates rapid washout of a substantial fraction of radioactivity from most organs during the 1- to 24-hr period after ^{131}I -IUdR administration. It is interesting to note substantial washout of radioactivity during the first 24 hr was observed for 16-day i.c. C6_m tumors (Group I studies) where a 10-fold differ-

TABLE 3
IUdR Uptake and Incorporation into DNA

Subcutaneous tumors	Total activity* (%dose/g tumor)		DNA activity* (%dose/g tumor)	DNA fraction
C6_a	0.49 \pm 0.13	0.45 \pm 0.11	0.928 \pm 0.014	

*Measured 24 hr after ^{131}I -IUdR administration; mean \pm s.d.; n = 6.

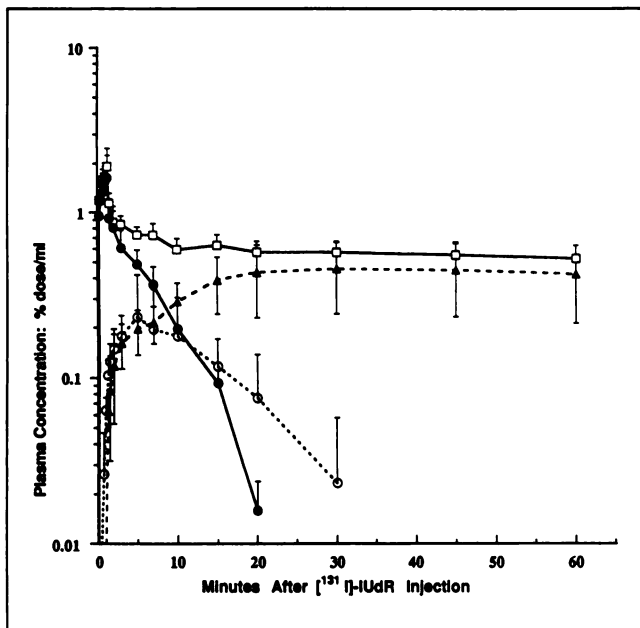


FIGURE 7. Time course of total plasma radioactivity (open square), parent ^{131}I -IUdR (closed circle), ^{131}I -iodide (closed diamond) and ^{131}I -iodouracil (open circle) following intravenous administration of ^{131}I -IUdR in Wistar rats.

ence between the 1-hr value and A_0 was observed. Conversely, most of the radioactivity measured in 8-day C6_m tumors at 1 hr was retained at 24 hr (Group III studies). The 1-hr-to- A_0 ratio was only 1.3, which indicates substantially less washout during the 1- to 24-hr period. This suggests a greater fraction of total radioactivity measured 1 hr after ^{131}I -IUdR administration was incorporated in DNA of 8-day compared to 16-day tumors. The clearance half-time of radioactivity from tumors and organ tissue was estimated from Day 1 to Day 4 or Day 5 (Table 4). Half-time values ranged from 26 to 67 hr for tumors and from 33 to 45 hr for different organs.

DISCUSSION

The clinical and biological manifestations of systemic and intracranial malignancy depend in part on the rate of tumor cell proliferation and the increase in tumor size. A quantitative estimate of tumor proliferative activity obtained through noninvasive medical imaging would aid in selecting optimal treatments for patients with tumors and could provide for an earlier and possibly a more accurate assessment of response to therapy and of prognosis. Carbon-11-labeled TdR has been proposed as a radiotracer for measuring tumor cell proliferation using PET by several groups (33-38). However, rapid metabolism and the appearance of radiolabeled metabolites of TdR in tissue as well as blood and the short physical half-life of ^{11}C present particular problems for measuring cell proliferation with ^{11}C -TdR and PET. For example, TdR labeled in the methyl group on the pyrimidine ring is rapidly metabolized in blood (36-38). Measurements of ^{11}C radioactivity in tumor and normal tissues within 1 hr of [methyl- ^{11}C]TdR admin-

istration include a large fraction of radiolabeled metabolites (37). Recently, it has been suggested that ^{11}C labeling of TdR on the 2 position of the pyrimidine ring results in fewer radiolabeled metabolites, although greater amounts of ^{11}C -carbon dioxide and related products are produced (39-41). A higher percentage of total tissue radioactivity was measured in the acid-insoluble or DNA fraction at 1 hr following injection of [2- ^{11}C]TdR compared to [methyl- ^{11}C]TdR injection (39-41). Nevertheless, the 20-min physical half-life of ^{11}C may be too short to allow for sufficient tissue washout and body clearance of the radiolabeled metabolites and will contribute to a comparatively high level of background radioactivity in the tumor and surrounding tissue.

A similar limitation exists with the use of ^{18}F -FUdR due to the 110-min physical half-life of ^{18}F . In the studies of Abe (7), ^{18}F -labeled pyrimidines were synthesized and visualization of ^{18}F -FUdR uptake in tumor by PET was attempted. Insufficient washout of background radioactivity due to ^{18}F -labeled metabolites in blood and surrounding tissues during the 1-hr period after intravenous administration of ^{18}F -FUdR limits its usefulness. In addition, ^{18}F -fluoride liberated by dehalogenation of FUdR is avidly accumulated by bone despite the fairly rapid excretion of fluoride by the kidney. Fluorine-18-FUdR is mainly a precursor of RNA synthesis (42) and the ^{18}F -FdUMP intermediate forms a complex with thymidilate synthetase that is acid insoluble (43).

Our interest in IUdR developed because long-lived radioisotopes of iodine are available for both PET and SPECT imaging. The comparatively long physical half-life of iodine radioisotopes will allow sufficient time for substantial washout of background radioactivity not incorporated into DNA prior to imaging. In addition, there is a large literature base that has developed over the past 30 yr on the use of halogenated pyrimidine nucleosides generally and on the clinical use of IUdR in particular. Halogenated pyrimidine nucleosides have been used to study the metabolic pathways of pyrimidine nucleoside incorporation into DNA and RNA and for measuring cell proliferation (11, 44-48, 59). Halogenated pyrimidine nucleosides have also been studied as potential chemotherapeutic agents (31, 44, 49-52) and have been used as radiation sensitizers (53-56) and as anti-viral agents (57, 58). Pharmacologic evaluation following intravenous administration of halogenated pyrimidines in humans was intensively studied in the early 1960s (13, 21, 30, 53) and more recently by Russo et al. and Klecker et al. (18, 32).

IUdR and bromodeoxyuridine (BrUdR) have been shown to have similar rates of incorporation into nuclear DNA during the S-phase of cell division and similar rates of dehalogenation; eighty percent of the administered dose is dehalogenated during the first 20 min after intravenous administration (14, 30, 44). The half-life of IUdR in plasma was shown to be less than 5 min and total body clearance to be about 0.75 liter/min/m² (18). The clearance of IUdR is higher than the clearance of most commonly used drugs in

TABLE 4
Tissue Clearance of ¹³¹I Radioactivity

Tissue	Group	Number of animals*	A ₀ [†] (%dose/g)	Clearance half-time [‡] (days)	R [§]	1-hr value [¶] (%dose/g)
Tumor						
C6 _a , i.c.	IV, V	22	0.48	1.6	0.92	—
C6 _a , s.c.	IV, V	22	0.64	1.4	0.80	—
C6 _m , i.c.	III	10	0.10	2.1	—	0.13 ± 0.07
C6 _m , i.c.	I	7	0.016	1.6	—	0.16 ± 0.01
Selected organs**						
Kidney	I, III, IV, V	39	0.154	1.9	0.91	0.59 ± 0.22
Lung	I, III, IV, V	39	0.132	1.7	0.81	0.32 ± 0.07
Liver	I, III, IV, V	39	0.079	1.9	0.83	0.27 ± 0.16
Heart	I, III, IV, V	39	0.045	1.6	0.95	0.22 ± 0.08
Testicle	I, III, IV, V	39	0.047	1.5	0.82	0.11 ± 0.09
Muscle	I, III, IV, V	39	0.024	1.4	0.95	0.17 ± 0.09
Cortex	I, III, IV, V	39	0.007	1.8	0.77	0.017 ± 0.002

*Number of animals in the 1- to 5-day fits of the data.

[†]Estimated tissue radioactivity at time zero from an exponential fit of the 1- to 5-day data.

[‡]Calculated from a single exponential fit of the 1- to 5-day tissue radioactivity data.

[§]Correlation coefficient.

[¶]The results of 1-hr experiments in two studies (Groups I and III); values are mean ± s.d., n = 7.

**The results from four separate studies (Groups I, III, IV and V) are combined since no postinoculation time-dependence was observed.

anticancer therapy, but is lower than that for other pyrimidines: for BrUdR, -1.9 liter/min/m² (28), for FUdR, -15 liter/min/m² (60) and for thymidine, 23 liter/min/m² (61). IUdR and BrUdR incorporated into DNA are fairly stable over several days (14, 44) before substantial removal by uracil-DNA glycolase occurs. Dehalogenation is the major step in the metabolic degradation of halogenated pyrimidine nucleotides, which may occur before or after the hydrolysis of the intermediate metabolite, 5-iodo-5,6-dihydrouracil (18, 22, 62). Liberated iodide is cleared rapidly by the kidney. More than 80% is excreted in the urine during the first 24 hr (13, 21, 22). Prior administration of KI or NaI can block radiolabeled iodine uptake by the thyroid, reduce endogenous iodination of tissue and plasma proteins and enhance the excretion of radiolabeled iodide by the kidney. Bromide liberated from BrUdR is cleared more slowly by the kidney than iodide and remains distributed in the extracellular fluid. Only 20% of bromide is excreted in the urine during the first 24 hr (30). This results in a higher background of bromide radioactivity compared to that of iodide and makes IUdR a better potential agent for in vivo imaging of tumor proliferative activity than BrUdR.

Sensitivity to Rate of Tumor Growth

IUdR uptake and retention values in C6_a tumors at various times after injection are comparable with previously reported values (14, 15, 19, 22, 44, 63). One of the issues that relates to the usefulness of IUdR as a potential imaging agent of tumor cell proliferation in clinical studies is the sensitivity of radioactivity measurements to differences in the rate of cell proliferation. To address this issue, we studied two different C6 cell lines with markedly different in vivo growth characteristics. Animals with i.c. C6_a tu-

mors had a mean survival of only 16 days. In contrast, i.c. and s.c. C6_m tumors were noted to grow more slowly and subsequently regressed in Wistar rats. Regression of C6_m tumors was noted after 21-28 days, presumably due to immunological rejection. As a measure of cell proliferation, we determined the change in volume of C6_m i.c. tumors in individual animals and demonstrated a time-dependent decrease in growth rate between 10 and 28 days after tumor inoculation (Fig. 4) and a time-dependent increase in the calculated tumor doubling time (Fig. 3). The decreasing growth rate and increasing doubling time of 8-, 10- and 16-day C6_m i.c. tumors corresponds to the decrease in the 24-hr uptake and retention of IUdR (Table 2). These results clearly demonstrate the sensitivity of IUdR uptake and retention to the time-dependent changes in growth rate of C6_m i.c. tumors.

Although the growth rate of C6_a i.c. tumors was not determined, it is likely to be substantially higher than that of C6_m i.c. tumors since the median survival of animals with C6_a i.c. tumors was only 16 days. The 24-hr uptake and retention of IUdR in C6_a tumors measured 10 and 11 days after i.c. inoculation of C6_a cells was more than 4-fold greater than that measured in C6_m tumors 8 days after i.c. inoculation of C6_m cells. It was more than 11-fold and 27-fold greater than that measured in C6_m tumors at 10 and 16 days after i.c. inoculation of C6_m cells. These results are consistent with a high growth rate of C6_a tumors and further indicate a relationship between the rate of cell proliferation and IUdR uptake and retention.

Tissue Background and Washout of Radioactivity

Plasma clearance of ¹³¹I radioactivity after intravenous administration of ¹³¹I-IUdR was biexponential and higher

than that described previously by Kriss et al. (30). More than 80% was cleared during the first 24 hr. Substantial washout of radioactivity was also observed in many organs and this is advantageous. Washout of organ radioactivity results in a low background for imaging primary and metastatic tumors at 24 or more hr after ^{131}I -IUdR administration. Radioactivity levels in subcutaneous and intracerebral tumors were similar to that measured in plasma 1 hr after IUdR injection. At 24 hr after injection, tumor activity was three to five times higher than that of plasma and 93% of tumor radioactivity was incorporated into DNA. The remaining 7% could be explained by equilibration of plasma radioactivity and extracellular tumor space of 20%–30%. Not surprisingly, skeletal muscle and normal brain reflect low background radioactivity that decreases at the same rate as plasma. The two log order difference in radioactivity between tumor and normal brain measured 48–96 hr after IUdR administration will provide high sensitivity for imaging tumors with PET and SPECT.

The reduction of tumor radioactivity after ^{131}I -IUdR administration could be due to a composite of several processes in addition to the “washout” of radiolabeled metabolites. One of them is DNA repair followed by deiodination of excised IUdR. Second, tumor cell death will result in DNA catabolism and deiodination of IUdR. Third, tumor growth between sequential measurements of tumor radioactivity will lead to a “dilution” of the measured value when expressed as radioactivity per gram of tumor tissue. A decrease in “concentration” due to tumor growth must be considered in evaluating the data, since incorporation of IUdR into DNA occurs in a single pulse (within 30–60 min of IUdR administration). We measured and expressed tumor radioactivity as a concentration rather than radioactivity per tumor in these studies because tumor size varied from animal to animal and because the time course of total radioactivity in single tumors could not be obtained using tissue sampling techniques. Due to the rapid clearance of IUdR from blood (Fig. 6), any increase in tumor cell mass during the 1- to 5-day postinjection period occurs without a corresponding increase in tumor radioactivity. Consequently, the measured tumor concentration (%dose/g tissue) will decrease even though total tumor radioactivity may remain constant in the tumor. To account for this “dilution” phenomena, we have modeled the effect of tumor growth on the measured concentration of radioactivity in the tissue (Fig. 8).

The increase in tumor volume is known to be exponential during the early stages of tumor growth and then assumes a nonexponential, more linear pattern of growth (29). To facilitate the analysis of IUdR uptake and retention in i.c. C6_m tumors, we showed that the increase in tumor volume could be described by the Gompertz equation (Fig. 3). These time-dependent changes in i.c. C6_m tumor growth and volume were used to calculate the “dilution effect” on tissue radioactivity (%dose/g tissue) for the 9- to 13-day postinoculation period (Group III) and the 17- to 21-day postinoculation period (Group I). The calculated tumor

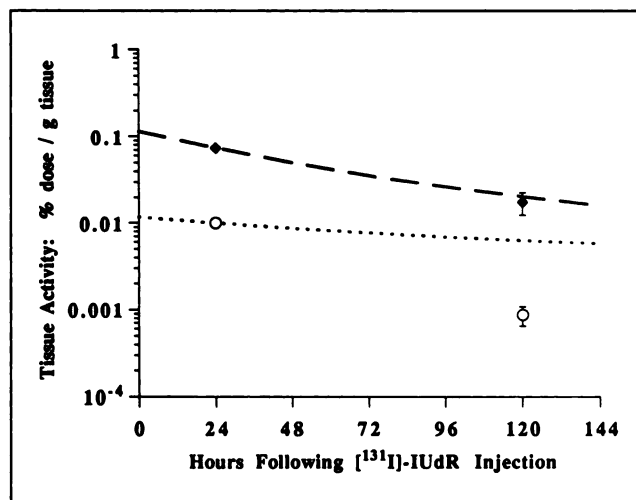


FIGURE 8. Modeling the effect of tumor growth on tissue radioactivity. Total radioactivity in the tumor was assumed to remain constant and the change in concentration, expressed as %dose/g of tissue, was assumed to be due to a “dilution effect” resulting from continued tumor growth and an increase in tumor volume after ^{131}I -IUdR incorporation into tumor DNA. For i.c. C6_m tumors, tumor growth and the increase in tumor volume could be described by the Gompertz equation (Fig. 3) and used to calculate a “dilution effect.” The lines represent estimated values of tissue activity (concentration, %dose/g of tumor) obtained from the model beginning 8 (dashed) and 16 (dotted) days, respectively, after i.c. C6_m tumor cell inoculation. Note that the estimated doubling times, 24 hr following ^{131}I -IUdR administration to animals with 8-day i.c. C6_m tumors (closed diamond; Group III) and with 16-day tumors (open circle; Group I) were substantially different: 2.4 and 4.2 days, respectively. The mean and s.d. of tissue activity actually measured are included for reference (Fig. 5).

concentration (%dose/g tissue) and apparent clearance of tissue radioactivity is shown by the dotted and dashed lines in Figure 7. Note that the decrease in tumor activity between 24 and 120 hr after ^{131}I -IUdR administration is consistent with tumor growth and a “dilution effect” during the 9- to 13-day postinoculation period (Group III), whereas the “dilution effect” of tumor growth does not account for the observed decrease in the 17- to 21-day postinoculation period (Group I). This suggests that alternative explanations are required to explain the observed decrease in tumor radioactivity in the Group I studies; two alternative explanations include tumor cell death and/or DNA repair. Tumor necrosis results in the release of radioactivity due to DNA breakdown and cleavage of iodine. Reutilization of IUdR during normal cell turnover is less than 10% (63). Data obtained by Lee et al. (27) suggest that there is a small probability for IUdR reutilization at the polynucleotide and nucleotide levels. Thymidine reutilization has been shown to be about 46% greater than IUdR (10). This level of IUdR recycling should not cause a significant error in estimating the pharmacokinetics of IUdR uptake and retention.

CONCLUSIONS

A noninvasive measurement of tumor cell proliferation would have immediate clinical utility. A measurement or image of IUdR incorporation into tumor DNA could aid in assessing grade of malignancy, contribute to treatment planning, provide an "early" assessment of treatment response prior to a change in tumor volume and could provide information that may relate to patient prognosis. The potential for the clinical application and use of IUdR tumor imaging in the future depends on two issues: (1) the relationship of IUdR-derived radioactivity measurements to other measurements of tumor cell proliferation and (2) the range of activities that can be imaged with PET and SPECT. In this study, we began to address the first issue. We showed that 93% of IUdR-derived ^{131}I radioactivity is in the DNA 24 hr after ^{131}I -IUdR administration and that there is a 40-fold difference in IUdR uptake and retention (24-hr values) between "rapidly growing" 10- to 11-day i.c. C₆_a and "slowly growing" 16-day i.c. C₆_m tumors. We also demonstrated that the time-dependent decrease in the growth rate of C₆_m tumors corresponds with a time-dependent decrease in IUdR uptake and retention.

Our results indicate that the use of longer-lived radioisotopes of iodine, such as ^{124}I for PET and ^{131}I or ^{123}I for SPECT, will be necessary for optimal imaging of $^*\text{I}$ -IUdR incorporation in tumor DNA. The use of longer-lived radioisotopes of iodine for labeling IUdR provides the opportunity for applying a time-dependent washout strategy with both PET and SPECT imaging. This reduces tissue background activity due to radiolabeled metabolites and increases imaging specificity to reflect IUdR DNA incorporation. This strategy is not possible with ^{11}C - and ^{18}F -labeled compounds.

ACKNOWLEDGMENTS

Parts of this study were presented at the 44th Annual Meeting of the American Academy of Neurology, San Diego, CA, 1992. Supported in part by DOE grant 86 ER60407.

REFERENCES

1. Rozental JM, Levine RL, Nickles RJ, Dobkin JA. Glucose uptake by gliomas after treatment. A positron emission tomographic study. *Arch Neurol* 1989;46:1302-1307.
2. Langen KJ, Roosen N, Kuwert T, et al. Early effects of intra-arterial chemotherapy in patients with brain tumors studied with PET: preliminary results. *Nucl Med Commun* 1989;10:779-790.
3. Ogawa T, Uemura K, Shishido F, et al. Changes of cerebral blood flow, oxygen and glucose metabolism following radiochemotherapy of gliomas: a PET study. *J Comput Assist Tomogr* 1988;12:290-297.
4. Mineura K, Yasuda T, Kowada M, Ogawa T, Shishido F, Uemura K. Positron emission tomographic evaluation of radiochemotherapeutic effect on regional cerebral hemocirculation and metabolism in patients with gliomas. *J Neuro Oncol* 1987;5:277-285.
5. Alavi JB, Alavi A, Goldberg HI, Dann R, Hickey W, Reivich M. Sequential computerized tomography and positron emission tomography studies in a patient with malignant glioma. *Nucl Med Commun* 1987;8:457-468.
6. Minuera K, Suda Y, Yasuda T, et al. Early and late stage positron emission tomography (PET) studies on the haemocirculation and metabolism of seemingly normal brain tissue in patients with gliomas following radiochemotherapy. *Acta Neurochirurgica* 1988;93:110-115.
7. Abe Y, Fukuda H, Ishiwata K, et al. Studies on ^{18}F -labeled pyrimidines. Tumor uptakes of ^{18}F -5-fluorouracil, ^{18}F -5-fluorouridine and ^{18}F -5-fluorodeoxyuridine in animals. *Eur J Nucl Med* 1983;8:258-261.
8. Vander Borgh T, Pauwels S, Shambotte L, Beckers C. Rapid synthesis of 2C-radiolabelled thymidine: a potential tracer for measurement of liver regeneration by PET [Abstract]. *J Nucl Med* 1989;30:929.
9. Strauss L, Dimitrakopoulou A, Clorius J, Schlag P, Helus F, Oberdorfer F. Fluorine-18-uracil uptake and changes in tumor volume during chemotherapy in patients with hepatic metastases from colorectal cancer [Abstract]. *J Nucl Med* 1989;30:911.
10. Dethlefsen L. Reutilization of ^{131}I -5-iodo-2'-deoxyuridine as compared to ^3H -thymidine in mouse duodenum and mammary tumor. *J Natl Cancer Inst* 1970;44:827-840.
11. Prusoff W. Incorporation of iododeoxyuridine, an analog of thymidine, into mammalian deoxyribonucleic acid. *Fed Proc* 1959;18:305.
12. Calabresi P, Cardoso S. Initial clinical studies with 5-iodo-2'-deoxyuridine. *Cancer Res* 1961;21:550-559.
13. Welch A, Jaffe J, Cardoso S. Studies on the pharmacology of 5-iododeoxyuridine in animals and man. *Cancer Res* 1960;3:161.
14. Hampton E, Eidinoff M. Administration of 5-iododeoxyuridine-I-131 in the mouse and rat. *Cancer Res* 1961;21:345-352.
15. Kriss J, Revesz L. The distribution and fate of bromodeoxyuridine and bromodeoxycytidine in the mouse and rat. *Cancer Res* 1962;22:254-265.
16. Hofer K, Prensly W, Hughes W. Death and metastatic distribution of tumor cells in mice monitored with ^{125}I -iododeoxyuridine. *J Natl Cancer Inst* 1969;43:763-773.
17. Dethlefsen L. Incorporation of ^{125}I -labeled 5-iodo-2'-deoxyuridine into the DNA of mouse mammary tumors. In: Fry PJM, ed. *Normal and malignant cell growth*. New York: Springer-Verlag; 1969:186-201.
18. Klecker Jr R, Jenkins J, Kinsella T, Fine R, Strong J, Collins J. Clinical pharmacology of 5-iodo-2'-deoxyuridine and 5-iodouracil and endogenous pyrimidine modulation. *Clin Pharmacol Ther* 1985;38:45-51.
19. Bagshawe K, Sharma S, Southall P, et al. Selective uptake of toxic nucleoside (^{125}I UdR) by resistant cancer. *Br J Radiol* 1991;64:37-44.
20. Humm J, Bagshawe K, Sharma S, Boxer G. Tissue dose estimates following the selective uptake of ^{125}I UdR and other radiolabeled thymidine precursors in resistant tumors. *Br J Radiol* 1991;64:45-49.
21. Calabresi P, Cardoso S, Finch S, et al. Initial clinical studies with 5-iodo-2'-deoxyuridine. *Cancer Res* 1961;21:550-559.
22. Prusoff W, Jaffe J, Gunther H. Studies in the mouse of the pharmacology of 5-iododeoxyuridine, an analogue of thymidine. *Biochem Pharmacol* 1960;3:110-121.
23. Benda P, Lightbody J, Sato G, Levine L, Sweet W. Differentiated rat glial cell strain in tissue culture. *Science* 1968;161:370-371.
24. Benda P, Someda K, Messer J, Sweet WH. Morphological and immunohistochemical studies of rat glial tumors and clonal strains propagated in cultures. *J Neurosurg* 1971;34:310-323.
25. Berger SB, Ballon D, Graham M, et al. Magnetic resonance imaging demonstrates that electric stimulation of cerebellar fastigial nucleus reduces cerebral infarction in rats. *MRI Stroke and Cerebellar Stimulation* 1990;21:172-176.
26. Mahmood U, Devitt ML, Kocheril PG, et al. Quantitation of total metastatic tumor volume in the rat liver: correlation of MR and histologic measurements. *JMRI* 1992;2:335-340.
27. Lee D, Prensly W, Krause G, Hughes W. Blood thymidine level and iododeoxyuridine incorporation and reutilization in DNA in mice given long-acting thymidine pellets. *Cancer Res* 1976;36:4577-4583.
28. Winsor CP. The Gompertz curve as a growth curve. *Proc Natl Acad Sci USA* 1932;18:1-7.
29. Steele GG. *Growth kinetics of tumors*. Oxford: Clarendon Press; 1977.
30. Kriss J, Maruyama Y, Tung L, Bond S, Revesz L. The fate of 5-bromodeoxyuridine, 5-bromodeoxycytidine and 5-iododeoxycytidine in man. *Cancer Res* 1963;23:260-268.
31. DeGroot LJ. Kinetic analysis of iodine metabolism. *J Clin Endocrinol* 1966;26:149.
32. Russo A, Gianni L, Kinsella T, et al. Pharmacological evaluation of intravenous delivery of 5-bromodeoxyuridine to patients with brain tumors. *Cancer Res* 1984;44:1702-1705.
33. Clarkson B, Ohkita T, Ota K, Fried J. Studies of cellular proliferation in human leukemia. I. Estimation of growth rates of leukemic and normal hematopoietic cells in two adults with acute leukemia given single injections of tritiated thymidine. *J Clin Invest* 1967;46:506-529.
34. Christman D, Crawford EJ, Friedkin M, et al. Detection of DNA synthesis in intact organisms with positron-emitting [methyl- ^{11}C]thymidine. *Proc Natl Acad Sci USA* 1972;69:988-992.
35. Larson SM, Weiden PL, Grunbaum Z, et al. Positron imaging feasibility

- studies. Characteristics of ^3H -thymidine uptake in rodent and canine neoplasms. *J Nucl Med* 1981;22:869–874.
36. Molnar P, Groothuis D, Blasberg R, Zaharko D, Owens E, Fenstermacher J. Regional thymidine transport and incorporation in experimental brain and subcutaneous tumors. *J Neurochem* 1984;43:421–432.
 37. Shields AF, Lim K, Grierson J, Link J, Krohn KA. Utilization of labeled thymidine in DNA synthesis: studies for PET. *J Nucl Med* 1990;31:337–342.
 38. Conti P, Grossman S, Wilson A, et al. Laboratory and clinical imaging studies of primary brain tumors using ^{11}C -thymidine positron emission tomography (PET) [Abstract]. *Proc Ann Meet Am Soc Clin Oncol* 1990;9:A357.
 39. Shields AF, Kozell LB, Link JM, Kozawa SM, Garmestani K. Comparison of PET imaging using C-11-thymidine labeled in the ring-2 and methyl positions [Abstract]. *J Nucl Med* 1990;31:794.
 40. Shields AF. Imaging tumor DNA synthesis with C-11 thymidine and positron emission tomography (PET) [Abstract]. *Cancer Res* 1990;31:205.
 41. Shields AF, Swenson ER, Bassingthwaite JB. Contribution of labeled carbon dioxide to PET imaging of C-11-labeled compounds [Abstract]. *J Nucl Med* 1992;33:581–586.
 42. Tsurumi Y, Kameyama M, Ishiwata K, et al. Fluorine-18-fluoro-2'-deoxyuridine as a tracer of nucleic acid metabolism in brain tumors. *J Neurosurg* 1990;72:110–113.
 43. Washiten WL, Santi DV. Assay of intracellular free and macromolecular-bound metabolites of 5-fluorodeoxyuridine and 5-fluorouracil. *Cancer Res* 1979;39:3397–3404.
 44. Eidinoff M, Cheong L, Rich M. Incorporation of unnatural pyrimidine bases into deoxyribonucleic acid of mammalian cells. *Science* 1959;129:1550–1551.
 45. Prusoff W. Synthesis and biological activities of iododeoxyuridine, an analog of thymidine. *Biochim et Biophys Acta* 1959;32:295–296.
 46. Krueger R, Gitlin D, Commerford S, Stein J, Hughes W. Iododeoxyuridine as a tracer of DNA metabolism in vivo. *Fed Proc* 1960;19:307.
 47. Xeros N. Deoxyriboside control and synchronization of mitosis. *Nature* 1962;194:682–683.
 48. Kufe D, Egan E, Rosowsky A, Ensminger W, Frei E. Thymidine arrest and synchrony of cellular growth in vivo. *Cancer Treat Rep* 1980;64:1307–1317.
 49. Mathias A, Fischer G, Prusoff W. Inhibition of the growth of mouse leukemia cells in culture by 5-iododeoxyuridine. *Biochim et Biophys Acta* 1959;36:560–561.
 50. Lee S, Giovanella B, Stehlin J. Effect of excess thymidine on the growth of human melanoma cells transplanted in thymus deficient nude mice. *Cancer Lett* 1977;3:209–214.
 51. Howell S, Chu B, Mendelsohn J, Carson D, Kung F, Seegmiller J. Thymidine as a chemotherapeutic agent: pharmacologic, cytokinetic and biochemical studies in a patient with T-cell acute lymphocytic leukemia. *J Natl Cancer Inst* 1980;65:277–284.
 52. Bruno S, Poster D, Bono V, MacDonald J, Kubota T. High-dose thymidine in clinical oncology. *Cancer Treat Rep* 1981;65:57–63.
 53. Djordjevic B, Szybalski W. Genetics of human cell lines III Incorporation of 5-bromo and 5-iododeoxyuridine into the deoxyribonucleic acid of human cells and its effect on radiation sensitivity. *J Exp Med* 1960;112:509–31.
 54. Kinsella T, Collins J, Rowland J, et al. Pharmacology and phase I/II study of continuous intravenous infusions of iododeoxyuridine and hyperfractionated radiotherapy in patients with glioblastoma multiforme. *J Clin Oncol* 1988;6:871–879.
 55. Lawrence T, Davis M, Maybaum J, Stetson P, Ensminger W. The dependence of halogenated pyrimidine incorporation and radiosensitization on the duration of drug exposure. *Int J Radiat Oncol Biol Phys* 1990;18:1393–1398.
 56. Sondak V, Lawrence T, Ensminger W, Chang A. Preoperative IUDR and radiation for soft tissue sarcomas: preliminary results and normal tissue IUDR incorporation data [Abstract]. *J Am Clin Oncol* 1990;9:A1228.
 57. Watanabe K, Reichman U, Hirota K, Lopez C, Fox J. Nucleosides 110 synthesis and antiherpes virus activity of some 2'-fluoro-2' deoxyarabino-furanosylpyrimidine nucleosides. *J Med Chem* 1979;22:21–24.
 58. Watanabe K, Su T, Klein R, et al. Nucleosides 123 synthesis of antiviral nucleosides: 5-substituted 1-(2-deoxy-2-halogeno- β -D-arabinofuranosyl)cytosines and -uracils. Some structure-activity relationships. *J Med Chem* 1983;28:152–156.
 59. Hoshino T, Nagashima T, Murovic J, et al. In situ cell kinetics studies on human neuroectodermal tumors with bromodeoxyuridine labeling. *J Neurosurg* 1986;64:453–459.
 60. Ensminger WD, Rosowsky A, Raso V, et al. A clinical-pharmacological evaluation of hepatic arterial infusions of 5-fluoro-2'-deoxyuridine and 5-fluorouracil. *Cancer Res* 1978;38:3784–3792.
 61. Howell SB, Ensminger WD, Krishan A, Frei E. Thymidine rescue of high-dose methotrexate in humans. *Cancer Res* 1978;38:325–330.
 62. Kim BD, Keenen S, Bodnar JK, Sander EG. Role of enzymatically catalyzed 5-iodo-5,6-dihydrouracil ring hydrolysis on the dehalogenation of 5-iodouracil. *J Biol Chem* 1976;251:6909–6914.
 63. Hughes W, Commerford S, Gitlin D, et al. Deoxyribonucleic acid metabolism in vivo. I. Cell proliferation and death as measured by incorporation and elimination of iododeoxyuridine. *Chem Med* 1964;23:640–648.